Effects of radiation damping on photorecombination of C^{4+} ions for the *KLL* resonance

Chuan-Ying Li,[1] Yong Wu,[1] Yi-Zhi Qu,[2] and Jian-Guo Wang[1,*]

[1]*Institute of Applied Physics and Computational Mathematics, P.O. Box 8009, Beijing 100088, People's Republic of China*

[2]*College of Material Sciences and Optoelectronic Technology, University of Chinese Academy of Sciences, Beijing 100049, China*

(Received 11 May 2016; published 3 October 2016)

A numerical method based on Zabaydullin and Dubau's work [O. Zabaydullin and J. Dubau, J. Phys. B: At. Mol. Opt. Phys. **45**, 115002 (2012)] has been developed to calculate the Cauchy principal value integral in scattering matrices and obtain photorecombination (PR) cross sections of low-lying resonances according to Davies and Seaton's theory [J. Phys. B **2**, 757 (1969)], in which radiation damping is included. The Dirac *R*-matrix method is employed to secure the dipole matrix. Using this method, PR cross sections of C^{4+} for the *KLL* resonance are acquired, and compared with available experimental measurements and other close-coupling theoretical results. It is shown that our damped cross sections reproduce the experimental data and are in agreement with other theoretical results. Meanwhile, radiation damping can reduce the PR cross section for the $1s2p^2\ ^2P$ resonance (corresponding to two levels $[(1s2p_{1/2})_1 2p_{3/2}]_{1/2}$ and $[1s(2p^2_{3/2})_2]_{3/2}$ by three orders of magnitude. The unresolved and underestimated resonances $1s2p^2\ ^4P$, $1s2s2p\ ^4P$, and $1s2p^2\ ^2P$ in the undamped Breit-Pauli *R*-matrix calculations [H. L. Zhang *et al.*, J. Phys. B: At. Mol. Opt. Phys. **32**, 1459 (1999)] are corrected. Besides, dielectronic recombination cross sections of C^{4+} for the *KLL* resonance are also presented for comparison using the relativistic configuration-interaction (RCI) method implemented in flexible atomic code (FAC), which show radiation damping has pronounced influences on $1s2p^2\ ^2P$ due to much larger radiative rates compared with autoionization rates. Furthermore, radiative and autoionization rates for the intermediate states $[(1s2p_{1/2})_1 2p_{3/2}]_{1/2}$ and $[1s(2p^2_{3/2})_2]_{3/2}$ of the He-like ions with $6 \leqslant Z \leqslant 83$ are calculated using FAC, scaling laws of which are checked. Autoionization rates comply with the $Z^0_{\rm eff}$ scaling law for $Z \geqslant 32$, which is caused by relativistic effects.

DOI: 10.1103/PhysRevA.94.042702

I. INTRODUCTION

Photorecombination (PR) is an atomic process of ongoing interest in applied and fundamental physics, due to its importance in influencing the ionization balance in hot plasmas and understanding the dynamics of the solar corona [1–5]. The PR cross sections and rate coefficients are vital for simulations of the radiative transfer and spectrum diagnosis in laboratory and astrophysical plasmas [6,7]. The PR process can proceed nonresonantly through radiative recombination (RR), which is a direct transition from a free to a bound state with a photon emitted. It can also proceed resonantly through dielectronic recombination (DR), which is a two-step electron-ion collision process, where at first a doubly excited intermediate state is created by a resonant dielectronic capture, and subsequently the intermediate state decays by photon emission. When both the initial state and the final state including the emitted photons are the same, RR and DR are indistinguishable, and the interference effects between them can generate asymmetric line profiles, as observed in storage-ring experiments [8,9], predicted earlier by preliminary radiation-damped *LS R*-matrix calculations [10], and further confirmed by multiconfiguration Breit-Pauli (MCBP) calculations extended to include interference effects [11,12].

To provide reliable PR data, in recent years an enormous amount of progress has been made in theories including perturbative and nonperturbative methods. The perturbative methods generally adopt the independent-process and isolated-resonance (IPIR) approximation [13,14], which treats RR and DR separately and neglects quantum mechanical interferences between the two and between DR resonances. Methods of this class are computationally more efficient and can include radiation damping (RD) [15,16] straightforwardly. However, they cannot be applied to theoretical modeling of asymmetric features associated with resonance-background and/or resonance-resonance interference effects, unless higher-order perturbative approaches are employed [11,12]. Nonperturbative approaches, like the close-coupling (CC) *R*-matrix methods, can automatically involve all orders of interferences, yet cannot take RD into account so easily as the perturbative ones. Using Davies and Seaton's (DS) [15] continuum-bound transition theory for including RD, Zhao *et al.* [17] developed a numerical method to calculate the low-lying resonance PR by directly evaluating the Cauchy principal value of the integral in scattering matrices, with the dipole matrix element calculated by the nonrelativistic *R*-matrix approach [18,19] in the *LS* coupling scheme. Robicheaux *et al.* [20] presented a radiative optical-potential approach for containing RD in the CC equations employing extensions of the *R*-matrix computer program RMATRX1 [19], where relativistic effects were included using the Breit-Pauli (BP) Hamiltonian. Based on this approach, many detailed PR calculations involving RD have been carried out for highly charged ions [21,22]. Also, an independent theoretical formulation addressing PR was developed by Zhang *et al.* [23,24], again using an extension of RMATRX1 with relativistic effects incorporated through the BP Hamiltonian. In their method, PR is divided into two groups: the low-n $n \leqslant n_0 \simeq 10$ one and the high-n $n_0 \leqslant n \leqslant \infty$ one. For the low-n group, PR cross sections are derived from photoionization cross sections through detailed balance (the Milne relation) [25] in the absence of RD. To include RD, the numerical scheme provided by Sakimoto *et al.* [26] should be used, which entails fitting the dipole matrices. For the high-n

*Corresponding author: wang_jianguo@iapcm.ac.cn

group, the radiation-damped S matrix derived by Bell and Seaton [27] is used in the analytic Gailitis averaging to secure PR cross sections, neglecting long-range channel coupling which may be important for getting the correct autoionization widths. Relativistic radiatively damped R-matrix calculations of electron-impact excitation were performed by Ballance and Griffin [28] and by Griffin and Ballance [29], where relativistic effects were incorporated using a modified parallel version of the Dirac R-matrix program DARC [30]. Dirac R-matrix PR calculations were carried out using the modified parallel version of DARC [28] for W^{35+} [31] and DARC for C^{4+} [32], respectively, in both of which PR cross sections were obtained from photoionization cross sections via detailed balance with RD neglected. To the authors' knowledge, there have been no other large-scale calculations of PR employing DARC.

In this paper, we develop a numerical method based on Zabaydullin and Dubau's work [33,34] to calculate the Cauchy principal value (PV) integral in the S matrix and obtain PR cross sections of low-lying resonances according to the DS theory, with RD included. A modified version of DARC [35] is employed to secure the dipole matrix. Using this method, PR cross sections of C^{4+} for the *KLL* resonance are acquired and compared with earlier experimental measurements [36], the nonrelativistic R-matrix results in LS coupling [17], as well as the relativistic BP R-matrix results [23]. The discrepancies between the undamped BP result and ours are discussed. Besides, to account for the influence of RD on the $1s2p^2\ ^2P$ resonance (corresponding to two levels $[(1s2p_{1/2})_1 2p_{3/2}]_{1/2}$ and $[1s(2p^2_{3/2})_2]_{3/2}$, with the subscript of the parenthesis representing the total angular momentum j), DR cross sections for the *KLL* resonance are given under the IPIR approximation using the relativistic configuration-interaction (RCI) method implemented in flexible atomic code (FAC) [37–39]. Furthermore, radiative transition probabilities A^r and autoionization rates A^a for the intermediate states $[(1s2p_{1/2})_1 2p_{3/2}]_{1/2}$ and $[1s(2p^2_{3/2})_2]_{3/2}$ of the He-like ions with $6 \leqslant Z \leqslant 83$ are calculated using FAC, the $Z^4_{\rm eff}$ and $Z^0_{\rm eff}$ scaling laws of which are examined, and the influences of relativistic effects and configuration interaction (CI) on A^r and A^a are discussed.

The remainder of this paper is organized as follows. In Sec. II, the theoretical methods employed in this study are described briefly. In Sec. III, our PR cross sections of C^{4+} obtained from the Dirac R-matrix method and the DR cross sections from the RCI method are presented and compared with earlier experimental and theoretical results. A^r and A^a for $[(1s2p_{1/2})_1 2p_{3/2}]_{1/2}$ and $[1s(2p^2_{3/2})_2]_{3/2}$ of the He-like ions with $6 \leqslant Z \leqslant 83$ are also given. Finally in Sec. IV, concluding remarks are drawn.

II. COMPUTATIONAL METHODS

A. DS theory

According to the DS theory [15], when interaction of the radiation field with the electron-ion system is included, a generalized electron-photon scattering matrix S may be obtained as

$$S = \begin{pmatrix} S_{ee} & S_{ep} \\ S_{pe} & S_{pp} \end{pmatrix}, \tag{1}$$

with S_{ee} the submatrix for electron scattering allowing for radiative decays, S_{pe} that for electron capture followed by the emission of a photon, S_{ep} that for photoionization, and S_{pp} that for photon-photon scattering. The PR submatrix S_{pe} is described as

$$S_{pe} = -2\pi i (1 + \mathbf{L})^{-1} \mathbf{D}^\dagger, \tag{2}$$

where $\mathbf{D}$ is the reduced dipole matrix in the form

$$\mathbf{D}_{\gamma J,\gamma' J'}(E) = \left(\frac{2\omega^3\alpha^3}{3\pi}\right)^{1/2} \frac{\langle \gamma J E \| \mathbf{R} \| \gamma' J' \rangle}{(2J+1)^{1/2}}, \tag{3}$$

and

$$\begin{aligned} \mathbf{L}(E) &= -i\pi \lim_{\tau\to 0} \int \frac{\mathbf{D}^\dagger(E')\mathbf{D}(E')}{E' - E - i\tau} dE' \\ &= \pi^2 \mathbf{D}^\dagger(E)\mathbf{D}(E) - i\pi \left[\mathrm{PV} \int \frac{\mathbf{D}^\dagger(E')\mathbf{D}(E')}{E' - E} dE' \right]. \end{aligned} \tag{4}$$

In Eq. (3), the continuum and the bound states are represented as γJE and $\gamma' J'$, respectively, with J and J' the corresponding total angular momenta, E the total energy of the continuum state, α the fine-structure constant, and ω the photon energy in units of hartrees. The wave function of the continuum electron is normalized per hartree.

Based on Zabaydullin and Dubau's work [33,34], the imaginary part of $\mathbf{L}(E)$ can be further expressed as

$$\mathbf{L}^{\rm Im}(E) = -\pi \lim_{R\to\infty} \int_{E-R}^{E+R} \frac{\mathbf{D}^\dagger(E')\mathbf{D}(E') - \mathbf{D}^\dagger(E)\mathbf{D}(E)}{E' - E} dE', \tag{5}$$

with the PV integral carried out numerically. A simple approximation of the DS theory called the ZD approximation was also presented in their work, in which the imaginary part of $\mathbf{L}(E)$ is neglected. The $\mathbf{L}$ matrix under this approximation is denoted by

$$\mathbf{L}^{\rm ZD}(E) = \pi^2 \mathbf{D}^\dagger(E)\mathbf{D}(E). \tag{6}$$

When $\mathbf{D}$ is small, i.e., $\mathbf{L} \simeq 0$, RD can be neglected and S_{pe} is approximated as

$$S_{pe} = -2\pi i \mathbf{D}^\dagger. \tag{7}$$

The PR probability for a given incident open channel j is given as

$$P_j^{\rm PR} = (1 - S_{ee}^\dagger S_{ee})_{jj} = (S_{pe}^\dagger S_{pe})_{jj}. \tag{8}$$

The total PR cross section is related to the PR probability as

$$\sigma^{\rm PR} = \frac{\pi}{2k^2 g} \sum_j g_j P_j^{\rm PR}, \tag{9}$$

where k^2 is the incident electron energy in units of Rydbergs; g and g_j are the statistical weights of the target and the continuum states, respectively.

B. Perturbative theory

Under the IPIR approximation, the DR cross section from an initial state i can be expressed as

$$\sigma(\epsilon) = \sum_d S_{id} L_d(\epsilon), \tag{10}$$

where

$$S_{id} = \frac{\pi^2}{\epsilon}\frac{g_d}{2g_i}\frac{A^a_{di}\sum_k A^r_{dk}}{\sum_{k'} A^r_{dk'} + \sum_{i'} A^a_{di'}}, \tag{11}$$

and

$$L_d(\epsilon) = \frac{(\Gamma_a + \Gamma_r)/(2\pi)}{(\epsilon - E_d)^2 + (\Gamma_a + \Gamma_r)^2/4}, \tag{12}$$

with all quantities given in atomic units. In Eq. (10), $L_d(\epsilon)$ is the Lorentzian line profile. In Eq. (11), ϵ is the incident electron energy; g_d and g_i are the statistical weights of the intermediate and the target states, respectively; $A^r_{dk'}$ is the radiative rate from the upper state d to the lower state k'; and $A^a_{di'}$ is the autoionization rate from the intermediate state d of the recombined ion to the i' state of the recombining ion. In Eq. (12), E_d is the resonance energy, and $\Gamma_a + \Gamma_r$ is the total width of the intermediate state d. When RD is small, the total width is approximated by the autoionization width, also $\sum_{k'} A^r_{dk'}$ in Eq. (11) is omitted.

III. RESULTS

In this section, we first present the Dirac R-matrix and RCI results of C^{4+} for the *KLL* resonance, and discuss the influence of RD on the $1s2p^2\ ^2P$ resonance. Second, radiative and autoionization rates for $[(1s2p_{1/2})_1 2p_{3/2}]_{1/2}$ and $[1s(2p^2_{3/2})_2]_{3/2}$ of the He-like ions with $6 \leqslant Z \leqslant 83$ are given, scaling laws of which are examined.

A. Dirac R-matrix and RCI results of C^{4+} for the *KLL* resonance

The PR process of C^{4+} for the *KLL* resonance can be described as

$$e^- + C^{4+}(1s^2) \rightarrow \begin{cases} C^{3+}(1s^2 2l) + h\nu & \text{(RR)}, \\ C^{3+}(1s2l2l') \rightarrow\ C^{3+}(1s^2 2l'') + h\nu & \text{(DR)}. \end{cases} \tag{13}$$

The Dirac R-matrix calculations are performed using our newly developed R-matrix programs [35], which comprise the internal region portions of DARC [30] and the external region parts of the traditional BP R-matrix code [19]. In order to integrate these two sets of programs, the Hamiltonian and the dipole matrix elements derived from the inner-region DARC code for a given $J\pi$ symmetry are reformatted to match those in the BP R-matrix code. The C^{4+} target wave functions are characterized by 16 orbitals consisting of nine physical orbitals $1s$, $2s$, $2p_{1/2}$, $2p_{3/2}$, $3s$, $3p_{1/2}$, $3p_{3/2}$, $3d_{3/2}$, and $3d_{5/2}$, along with seven pseudo-orbitals $\overline{4s}$, $\overline{4p_{1/2}}$, $\overline{4p_{3/2}}$, $\overline{4d_{3/2}}$, $\overline{4d_{5/2}}$, $\overline{4f_{5/2}}$, and $\overline{4f_{7/2}}$. All these orbitals are yielded by the relativistic self-consistent field (RSCF) calculation of the multiconfiguration Dirac-Fock code GRASP2K [40] using an extended optimized level (EOL) scheme for the lowest 17 levels, with the configuration bases arising from all the single and double promotions from six reference configurations including $1s^2$, $1s2s$, $1s2p$, $1s3s$, $1s3p$, and $1s3d$ to the $n = 4$ orbitals. In the scattering calculations, the lowest 17 levels of C^{4+} are included in the close-coupling expansion, with the same configuration bases as those in the RSCF calculations.

TABLE I. Lowest 17 energy levels of C^{4+} in Rydbergs. Δ denotes the percentage difference between our result and the NIST value.

Level	J	This work	NIST data	Δ
$1s^2$	0	0	0	
$1s2s$	1	21.950	21.973	–0.11%
$1s2s$	0	22.356	22.372	–0.07%
$1s2p_{1/2}$	1	22.350	22.373	–0.10%
$1s2p_{1/2}$	0	22.349	22.373	–0.11%
$1s2p_{3/2}$	2	22.351	22.374	–0.10%
$1s2p_{3/2}$	1	22.610	22.630	–0.09%
$1s3s$	1	25.853	25.876	–0.09%
$1s3s$	0	25.964	25.982	–0.07%
$1s3p_{1/2}$	1	25.960	25.984	–0.09%
$1s3p_{1/2}$	0	25.960	25.984	–0.09%
$1s3p_{3/2}$	2	25.961	25.984	–0.09%
$1s3d_{3/2}$	1	26.014	26.038	–0.09%
$1s3d_{3/2}$	2	26.014	26.038	–0.09%
$1s3d_{5/2}$	3	26.014	26.038	–0.09%
$1s3d_{5/2}$	2	26.016	26.040	–0.09%
$1s3p_{3/2}$	1	26.035	26.056	–0.08%

Our calculated energy levels are in excellent agreement with the NIST data [41] within ~0.1% as listed in Table I.

All the scattering calculations are performed with 40 continuum basis functions and a boundary radius of 8.4 Bohr radii. The theoretical energies of C^{4+} are adjusted to match experimental values in the diagonalization process of the Hamiltonian matrix in order that the resonance positions can be improved. To resolve narrow resonances, a suitably chosen fine energy mesh of 5 μeV is employed. Since dipole selection rules apply, the bound-free dipole matrices, $J^\pi = 1/2^e \rightarrow J'^{\pi'} = 1/2^o, 3/2^o$, $J^\pi = 1/2^o \rightarrow J'^{\pi'} = 1/2^e, 3/2^e$, and $J^\pi = 3/2^o \rightarrow J'^{\pi'} = 1/2^e, 3/2^e, 5/2^e$ are calculated to obtain the associated PR submatrices via Eq. (2); subsequently the total PR cross sections for the *KLL* resonance are derived through Eq. (9).

Comparison of our detailed PR cross sections for the *KLL* resonance with other R-matrix results is presented in Fig. 1. Figure 1(a) displays the nonrelativistic R-matrix results with RD in *LS* coupling from Ref. [17], Fig. 1(b) displays the BP R-matrix results with and without RD from Ref. [23], and Fig. 1(c) displays our Dirac R-matrix results in length formulations. Since our cross sections in length and velocity formulations are in excellent agreement with each other, only the length results are shown. Due to the conservation of total spin angular momentum and lack of an even-parity continuum state ^2P to interact with, DR via the $1s2s2p\ ^4P$, $1s2p^2\ ^4P$, and $1s2p^2\ ^2P$ resonances is forbidden in *LS* coupling, which should arise when relativistic effects are included. However, only the $1s2p^2\ ^2P$ resonance appears in the BP R-matrix results, which is obviously underestimated in the undamped result, due to the coarse energy mesh (in the order of meV) adopted in their calculations. Our Dirac R-matrix calculations show RD can reduce the PR cross section for the $1s2p^2\ ^2P$ resonance by three orders of magnitude. Also shown in Fig. 1(c) is the PR cross section under the ZD approximation [33,34]. It is shown that this approximation is

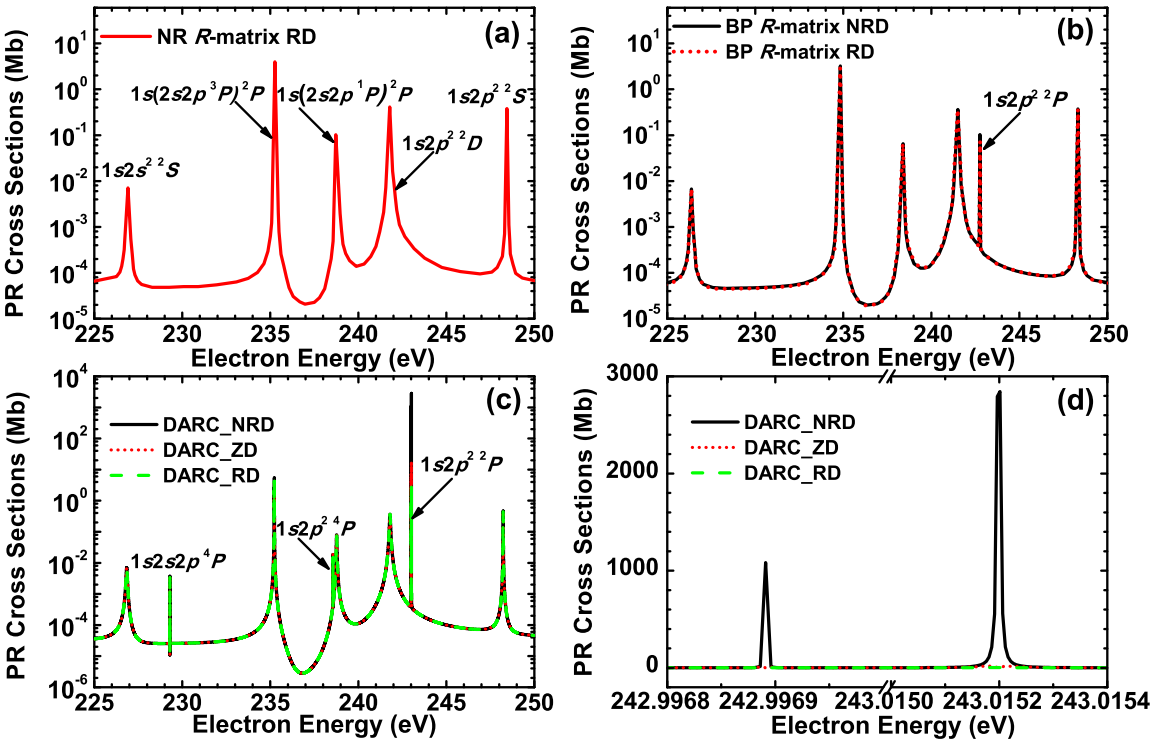

FIG. 1. Comparison of our detailed PR cross sections for the *KLL* resonance of C^{4+} with other *R*-matrix results. (a) The nonrelativistic *R*-matrix results with RD in *LS* coupling from Ref. [17]. (b) The BP *R*-matrix results with (red dotted curve) and without (black solid curve) RD from Ref. [23]. (c) The Dirac *R*-matrix results with RD (green dashed curve), under the ZD approximation (red dotted curve), and without RD (black solid curve). (d) The Dirac *R*-matrix results for the $1s2p^2\ ^2P$ resonance appearing at about 243 eV in (c). Symbols in (d) have the same meanings as those in (c).

reasonable and can include most of the RD effects, requiring much less computation effort. In Fig. 1(d) our Dirac *R*-matrix results for the $1s2p^2\ ^2P$ resonance, appearing at about 243 eV in Fig. 1(c), are shown separately to highlight the RD effect.

Comparison of our convolved PR cross sections for the *KLL* resonance with other *R*-matrix results and the experimental spectrum [36] is shown in Fig. 2. All the theoretical cross sections have been convoluted with a Gaussian distribution of 0.57 eV FWHM in order to compare directly with the experimental measurements. Since relativistic effects are weak for C^{4+} ions, the $1s2s2p\ ^4P$, $1s2p^2\ ^4P$, and $1s2p^2\ ^2P$ resonances are too narrow to be resolved by the experiment, the former two of which also disappear in our results. However, in contrast to the BP results, the $1s2p^2\ ^2P$ resonance should appear in a relativistic undamped cross section and disappear in a damped result due to RD, as shown in Fig. 2(c). In addition, the resonance positions in our Dirac *R*-matrix results are in better agreement with the experimental data than those in the BP *R*-matrix results, indicating that the electron correlation and interchannel coupling effects are treated appropriately.

Since the perturbative theoretical approach can incorporate RD straightforwardly, the RCI DR cross sections for the *KLL* resonance obtained using FAC are also given to account for the influence of RD on the $1s2p^2\ ^2P$ resonance, and compared with the result derived using a revised simplified relativistic configuration-interaction (SRCI) method [42] as well as the experiment spectrum, as displayed in Fig. 3. It should be pointed out that Bautista and Badnell made a similar comparison to the same experiment in the perturbative

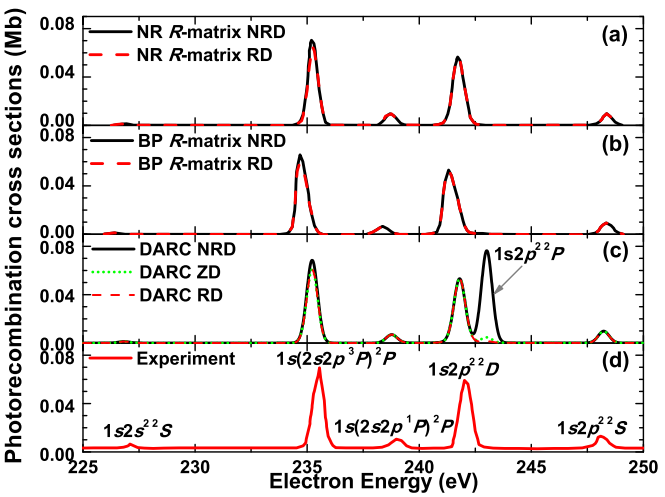

FIG. 2. Comparison of our convolved PR cross sections for the *KLL* resonance of C^{4+} with other *R*-matrix results and the experimental spectrum. (a) The nonrelativistic *R*-matrix results with (red dashed curve) and without (black solid curve) RD in *LS* coupling from Ref. [17]. (b) The BP *R*-matrix results with (red dashed curve) and without (black solid curve) RD from Ref. [23]. (c) The Dirac *R*-matrix results with RD (red dashed curve), under the ZD approximation (green dotted curve), and without RD (black solid curve). (d) The experimental spectrum from Ref. [36]. All the theoretical cross sections have been convoluted with a Gaussian distribution of 0.57 eV FWHM.

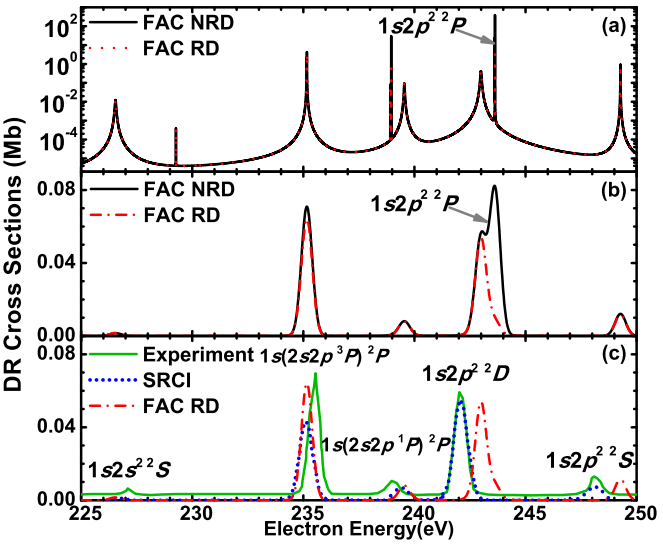

FIG. 3. Comparison of our RCI DR cross sections for the *KLL* resonance of C^{4+} with the SRCI results from Ref. [42] and the experimental spectrum from Ref. [36]. (a) Our detailed DR cross sections with (red dotted curve) and without (black solid curve) RD. (b) The DR cross sections convoluted with a Gaussian distribution of 0.57 eV FWHM with (red dash dotted curve) and without (black solid curve) RD. (c) Comparison of the convolved DR cross sections including RD (red dash dotted curve) with the SRCI results (blue short dotted curve) and the experimental spectrum (green solid curve).

AUTOSTRUCTURE calculations, and obtained good agreement with the measurement [43]. Since DR rate coefficients instead of cross sections for the *KLL* resonance were provided in their work, their results are not shown here. In our RCI calculations, CI within the same n complex is taken into account, which is the same as that in Ref. [42]. For $[(1s2p_{1/2})_1 2p_{3/2}]_{1/2}$ and $[1s(2p^2_{3/2})_2]_{3/2}$, the calculated total radiative rates 1.177×10^{12} and 1.176×10^{12} s^{-1} are much larger than the corresponding autoionization rates 1.934×10^7 and 1.215×10^{11} s^{-1}, which accounts for the pronounced effect of RD on $1s2p^2\ ^2P$ [see Figs. 3(a) and 3(b)]. In addition, our RCI damped cross section is in reasonable agreement with the SRCI result and the experimental spectrum [see Fig. 3(c)].

B. Radiative and autoionization rates for $[(1s2p_{1/2})_1 2p_{3/2}]_{1/2}$ and $[1s(2p^2_{3/2})_2]_{3/2}$ of the He-like ions with $6 \leqslant Z \leqslant 83$

Radiative and autoionization rates for $[(1s2p_{1/2})_1 2p_{3/2}]_{1/2}$ and $[1s(2p^2_{3/2})_2]_{3/2}$ of the He-like ions with $6 \leqslant Z \leqslant 83$ are presented in Fig. 4. It is shown that radiative rates are orders of magnitude larger than the corresponding autoionization rates along the isoelectronic sequence. Autoionization rates scale as $Z^0_{\rm eff}$ rigorously for hydrogenic ions, which is approximately true even for multielectron ions [25]. However, in this isoelectronic sequence, autoionization rates for both $[(1s2p_{1/2})_1 2p_{3/2}]_{1/2}$ and $[1s(2p^2_{3/2})_2]_{3/2}$ rise considerably up to orders of magnitude till $Z = 32$ (the corresponding element symbol Ge is marked), then keep a nearly constant value with increasing Z. Due to lack of an even-parity continuum state ^2P to interact with, autoionization from $1s2p^2\ ^2P$ is forbidden in *LS* coupling, which induces the small autoionization rates

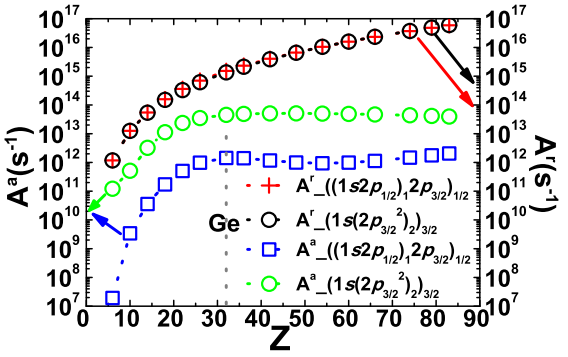

FIG. 4. Autoionization and total radiative rates for $[(1s2p_{1/2})_1 2p_{3/2}]_{1/2}$ and $[1s(2p^2_{3/2})_2]_{3/2}$ of the He-like ions with $6 \leqslant Z \leqslant 83$.

for the low-Z ions. As relativistic effects increase with Z, *LS* coupling is no longer appropriate and the coupling conditions approach pure *jj* coupling, then autoionization rates become independent of $Z_{\rm eff}$.

Radiative rates divided by $Z^4_{\rm eff}$ for $[(1s2p_{1/2})_1 2p_{3/2}]_{1/2}$ and $[1s(2p^2_{3/2})_2]_{3/2}$ of the He-like ions with $6 \leqslant Z \leqslant 83$ are exhibited in Fig. 5. Radiative rates for $\Delta n \neq 0$ transitions scale as $Z^4_{\rm eff}$ in the hydrogenic approximation [25]. The maxima of radiative rates divided by $Z^4_{\rm eff}$ for the $[(1s2p_{1/2})_1 2p_{3/2}]_{1/2} - 1s^2 2p_{1/2}$ and $[(1s2p_{1/2})_1 2p_{3/2}]_{1/2} - 1s^2 2p_{3/2}$ transitions are around 3 times the minima in the isoelectronic sequence. Thus the radiative rates for these two transitions and the total radiative rates for $[(1s2p_{1/2})_1 2p_{3/2}]_{1/2}$ scale as $Z^4_{\rm eff}$ approximately [see Fig. 5(a)]. Radiative rates for the $[1s(2p^2_{3/2})_2]_{3/2} - 1s^2 2p_{3/2}$ transition also scale as $Z^4_{\rm eff}$ approximately. But those for the $[1s(2p^2_{3/2})_2]_{3/2} - 1s^2 2p_{1/2}$ transition decrease rapidly with increasing Z, and violate the $Z^4_{\rm eff}$ scaling law [see Fig. 5(b)], which is caused by relativistic effects and CI. The coupling condition for the $[1s(2p^2_{3/2})_2]_{3/2}$ state changes from *LS* coupling at low Z to nearly pure *jj* coupling at high Z, due to the Z-scaling competition between the Coulombic coupling between electrons and the spin-orbit coupling. At large Z, the spin-orbit interactions dominate and relativistic effects become significant. Figure 6 exhibits the square of the mixing coefficient for each basis of $[1s(2p^2_{3/2})_2]_{3/2}$ along the isoelectronic sequence calculated using FAC to indicate the change of the coupling scheme. The two bases $[(1s2p_{1/2})_0 2p_{3/2}]_{3/2}$ and $[(1s2p_{1/2})_1 2p_{3/2}]_{3/2}$ contribute to the $[1s(2p^2_{3/2})_2]_{3/2} - 1s^2 2p_{1/2}$ transition, which is permitted with CI included. The squares of the mixing

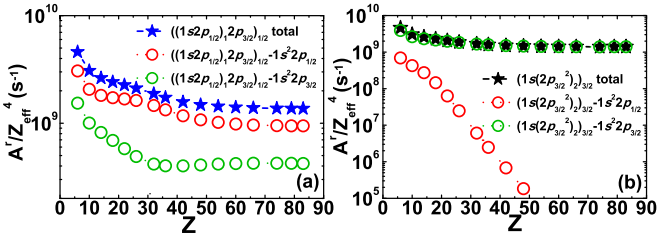

FIG. 5. $A^r/Z^4_{\rm eff}$ for (a) $[(1s2p_{1/2})_1 2p_{3/2}]_{1/2}$ and (b) $[1s(2p^2_{3/2})_2]_{3/2}$ of the He-like ions with $6 \leqslant Z \leqslant 83$.

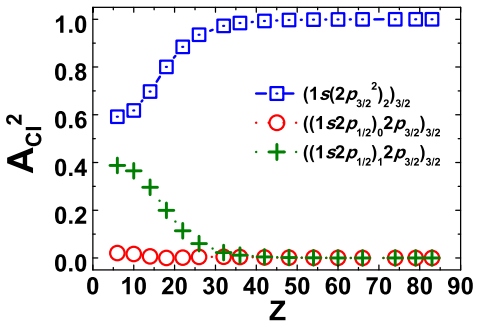

FIG. 6. Square of the mixing coefficient for each basis of $[1s(2p_{3/2}^2)_2]_{3/2}$ of the He-like ions with $6 \leqslant Z \leqslant 83$.

coefficients for the two bases, which represent the percentages of the bases involved in the intermediate state, diminish rapidly to zero with increasing Z, leading to the decrease in radiative rates.

IV. CONCLUSIONS

To summarize, we have developed a numerical method based on Zabaydullin and Dubau's work in combination with the DS theory to calculate the PV integral in scattering matrices and obtain PR cross sections of low-lying resonances, with the dipole matrix secured using the Dirac R-matrix code. This method can naturally involve RD as well as the resonance-background and/or resonance-resonance interference effects. Besides, the Dirac R-matrix method can include more detailed resonant structures compared to the nonrelativistic R-matrix approach. Using this method, PR cross sections of C^{4+} for the KLL resonance are acquired. Comparison of the present damped results with available experimental and theoretical results demonstrates the reliability of our method. Also, the ZD approximation is evaluated and proves to be reasonable. It is shown that RD can reduce the PR cross section for the $1s2p^2\,^2P$ resonance by three orders of magnitude. The RCI results show that RD has a pronounced influence on the $1s2p^2\,^2P$ resonance due to much larger radiative rates compared with autoionization rates. Furthermore, radiative and autoionization rates for $[(1s2p_{1/2})_1 2p_{3/2}]_{1/2}$ and $[1s(2p_{3/2}^2)_2]_{3/2}$ of the He-like ions with $6 \leqslant Z \leqslant 83$ are calculated using FAC. It is noted that autoionization rates comply with the $Z_{\rm eff}^0$ scaling law for $Z \geqslant 32$, which is caused by relativistic effects.

ACKNOWLEDGMENTS

This work was supported by the National Basic Research program of China under Grant No. 2013CB922200, by the National Natural Science Foundation (NSFC) of China under Grants No. 11405010, No. 11474032, No. 11474031, No. 11275029, and No. 11534011, by the foundation of President of Chinese Academy of Engineering Physics Grant No. 2014-1-029, and by the Foundation for Development of Science and Technology of China Academy of Engineering Physics under Grants No. 2013A0102005 and No. 2014A0102005.

[1] A. Burgess, Astrophys. J. **139**, 776 (1964).
[2] N. R. Badnell, C. P. Ballance, D. C. Griffin, and M. O'Mullane, Phys. Rev. A **85**, 052716 (2012).
[3] K. Spruck, N. R. Badnell, C. Krantz, O. Novotný, A. Becker, D. Bernhardt, M. Grieser, M. Hahn, R. Repnow, D. W. Savin, A. Wolf, A. Müller, and S. Schippers, Phys. Rev. A **90**, 032715 (2014).
[4] U. I. Safronova, A. S. Safronova, and P. Beiersdorfer, Phys. Rev. A **91**, 062507 (2015).
[5] V. V. Flambaum, M. G. Kozlov, and G. F. Gribakin, Phys. Rev. A **91**, 052704 (2015).
[6] R. K. Janev, L. P. Presnyakov, and V. P. Shevelko, *Physics of Highly Charged Ions* (Springer, Berlin, 1985).
[7] H. P. Summers, Adv. At. Mol. Opt. Phys. **33**, 275 (1994).
[8] S. Schippers, T. Bartsch, C. Brandau, G. Gwinner, J. Linkemann, A. Muller, A. A. Saghiri, and A. Wolf, J. Phys. B: At. Mol. Opt. Phys. **31**, 4873 (1998).
[9] S. Schippers, S. Kieslich, A. Muller, G. Gwinner, M. Schnell, A. Wolf, A. Covington, M. E. Bannister, and L.-B. Zhao, Phys. Rev. A **65**, 042723 (2002).
[10] T. W. Gorczyca, M. S. Pindzola, F. Robicheaux, and N. R. Badnell, Phys. Rev. A **56**, 4742 (1997).
[11] D. Nikolic, T. W. Gorczyca, and N. R. Badnell, Phys. Rev. A **79**, 012703 (2009).
[12] D. Nikolic, T. W. Gorczyca, and N. R. Badnell, Phys. Rev. A **81**, 030501 (2010).
[13] M. S. Pindzola, N. R. Badnell, and D. C. Griffin, Phys. Rev. A **46**, 5725 (1992).
[14] D. H. Kwon and D. W. Savin, Astrophys. J. **734**, 2 (2011).
[15] P. C. W. Davies and M. J. Seaton, J. Phys. B **2**, 757 (1969).
[16] N. R. Badnell, T. W. Gorczyca, and A. D. Price, J. Phys. B: At. Mol. Opt. Phys. **31**, L239 (1998).
[17] L.-B. Zhao, A. Ichihara, and T. Shirai, Phys. Rev. A **62**, 022706 (2000).
[18] P. G. Burke, A. Hibbert, and W. D. Robb, J. Phys. B **4**, 153 (1971).
[19] K. A. Berrington, W. B. Eissner, and P. H. Norrington, Comput. Phys. Commun. **92**, 290 (1995).
[20] F. Robicheaux, T. W. Gorczyca, M. S. Pindzola, and N. R. Badnell, Phys. Rev. A **52**, 1319 (1995).
[21] T. W. Gorczyca, F. Robicheaux, M. S. Pindzola, and N. R. Badnell, Phys. Rev. A **54**, 2107 (1996).
[22] T. W. Gorczyca, N. R. Badnell, and D. W. Savin, Phys. Rev. A **65**, 062707 (2002).
[23] H. L. Zhang, S. N. Nahar, and A. K. Pradhan, J. Phys. B: At. Mol. Opt. Phys. **32**, 1459 (1999).
[24] H. L. Zhang, S. N. Nahar, and A. K. Pradhan, Phys. Rev. A **64**, 032719 (2001).
[25] R. D. Cowan, *Atomic Structure and Spectra* (University of California, Los Angeles, 1981).
[26] K. Sakimoto, M. Terao, and K. A. Berrington, Phys. Rev. A **42**, 291 (1990).
[27] R. H. Bell and M. J. Seaton, J. Phys. B **18**, 1589 (1985).
[28] C. P. Ballance and D. C. Griffin, J. Phys. B: At., Mol. Opt. Phys. **39**, 3617 (2006).

[29] D. C. Griffin and C. P. Ballance, J. Phys. B: At., Mol. Opt. Phys. **42**, 235201 (2009).
[30] P. H. Norrington, http://www.am.qub.ac.uk/darc.
[31] C. P. Ballance, S. D. Loch, M. S. Pindzola, and D. C. Griffin, J. Phys. B: At. Mol. Opt. Phys. **43**, 205201 (2010).
[32] K. Ma, L.-Y. Xie, D.-H. Zhang, and C.-Z. Dong, Chin. Phys. B **24**, 073402 (2015).
[33] O. Zabaydullin and J. Dubau, J. Phys. B: At. Mol. Opt. Phys. **45**, 115002 (2012).
[34] O. Zabaydullin and J. Dubau, J. Phys. B: At. Mol. Opt. Phys. **46**, 075005 (2013).
[35] C.-Y. Li, X.-Y. Han, J.-G. Wang, and Y.-Z. Qu, Chin. Phys. B **22**, 123201 (2013).
[36] S. Mannervik, S. Asp, L. Brostrom, D. R. DeWitt, J. Lidberg, R. Schuch, and K. T. Chung, Phys. Rev. A **55**, 1810 (1997).
[37] M. F. Gu, Astrophys. J. **582**, 1241 (2003).
[38] M. F. Gu, Astrophys. J. **589**, 1085 (2003).
[39] M. F. Gu, Astrophys. J. **590**, 1131 (2003).
[40] P. Jonsson, X. He, C. Froese Fischer, and I. P. Grant, Comput. Phys. Commun. **177**, 597 (2007).
[41] A. Kramida, Y. Ralchenko, J. Reader, and N. A. Team, NIST Atomic Spectra Database, Ver. 5.2, 2014.
[42] Y.-Q. Xu, Y.-Z. Qu, X.-H. Zhang, and J.-M. Li, Phys. Rev. A **62**, 022715 (2000).
[43] M. A. Bautista and N. R. Badnell, Astron. Astrophys. **466**, 755 (2007).